Article:
Hardwick, L. orcid.org/0000-0003-0801-125X, Webb, P. and Goodall, R. orcid.org/0000-0003-0720-9694 (2023) Design of higher temperature copper brazing filler metals with reduced brittle phase content. Materials Today Communications, 35. 105524. ISSN: 2352-4928

https://doi.org/10.1016/j.mtcomm.2023.105524

Materials Today Communications 35 (2023) 105524

Contents lists available at ScienceDirect

Materials Today Communications

journal homepage: www.elsevier.com/locate/mtcomm

Design of higher temperature copper brazing filler metals with reduced brittle phase content

Liam Hardwick [a,*], Phil Webb [b], Russell Goodall [a]

[a] Department of Materials Science & Engineering, University of Sheffield, Sheffield S1 3JD, United Kingdom
[b] VBC Group, Castle Business Park, Loughborough LE11 5GW, United Kingdom

ARTICLE INFO

Keywords:
Metals and alloys
Intermetallics
Microstructure
SEM

ABSTRACT

Anneal-resistant copper alloys have been developed to address the need for stronger yet lighter fin and tube parts in heat exchangers, in order to facilitate greater efficiency and increased temperature capability. As such, brazing as opposed to traditional soldering has become the preferred joining method for these materials, due to the enhanced high-temperature properties of such joints. Copper-based filler metals are used extensively for the brazing of these materials, generally based on the copper-phosphorus system with alloying additions. In the present study, the microstructural issues arising from the current commercially available filler metals are discussed and addressed through CALPHAD-supported alloy design. Three selected novel compositions were used in the brazing of pure copper as a test of the design concept. Alloy compositions in weight percent of Cu(bal.)– 7Ni-4Sn-5 P and Cu(bal.)-10Ni-2Sn-6.5 P were found to result in a reduction of brittle Cu_3P phase while increasing the fraction (0.78 and 0.77 respectively) of copper-rich solid solution in joints post-braze, comparing favourably to commercial Meta-Braze™ 077 under similar conditions (0.61). Furthermore, the copper-rich solid solution was leaner in tin, predicted to impart an increased melting temperature while microhardness profiles indicate increased joint ductility. The implications for mechanical properties of filler metals in this alloy family are discussed.

1. Introduction

Heat exchangers are crucial systems for both heating and cooling in numerous industries such as energy, petrochemical and automotive. Copper and brass alloys have long been important materials in their manufacture, due to the combination of properties such as thermal conductivity, corrosion resistance, tensile strength and ductility [1,2]. Due to the detrimental annealing effects on the strength of these alloys, soldering (at below 450 °C) was the preferred method for joining sheets and fins of copper and brass alloys in heat exchangers [3,4]. More recently, stronger copper alloys were developed to satisfy industry demand for lighter, thinner tubes and fins for heat exchanger construction, increasing efficiency of heat transfer due to the smaller cross-sectional area [3,4].

The development of anneal-resistant chromium-containing copper alloys allowed the application of brazing as the joining method in heat exchanger fabrication, producing stronger joints capable of withstanding elevated temperatures as compared to soldering. For example, the CuproBraze® technology [5] utilises brazing for producing heat exchangers in demanding automotive engine applications. As opposed to soldering, brazing is defined as being conducted at temperatures above 450 °C, but the two are fundamentally similar. A filler metal is selected whose melting temperature is below that of the solidus of the base material (metal or ceramic) being joined, and upon melting this flows and fills the gap through capillary action and interacts with and partially dissolves base material close to the interface. Upon cooling, a metallic joint is thus formed.

Melting point depressing (MPD) elements are common alloying additions in brazing filler metals (for example, boron and silicon in nickel-based brazing alloys [6,7]) so that the onset of melting occurs at a suitable temperature, which may be far, or as little as 20–50 °C, below the solidus of the base material being joined. Copper-based filler metals, such as those used to join copper alloys in heat exchangers, generally contain phosphorus with contents of several weight percent [8,9]. The presence of phosphorus helps to reduce the filler metal melting temperature, but also improves the wetting and flow characteristics, and as such Cu-P filler metals are generally self-fluxing [9,10], which alleviates potential corrosion form flux residue [11]. Traditionally, copper-based

* Corresponding author.
E-mail addresses: liam.hardwick@sheffield.ac.uk (L. Hardwick), phil.webb@vbcgroup.com (P. Webb), r.goodall@sheffield.ac.uk (R. Goodall).

https://doi.org/10.1016/j.mtcomm.2023.105524
Received 1 September 2022; Received in revised form 27 December 2022; Accepted 29 January 2023
Available online 31 January 2023

filler metals would be either Cu-P binary filler metals or Cu-Ag-P filler metals; the former may have P content of between approximately 5 and 8 wt%, with solidus temperature of 710 °C and liquidus temperatures of up to approximately 890 °C [12] (here the steepness of the liquidus lines around the eutectic composition is noted [13]); the latter may have similar P contents, along with a range of Ag contents between approximately 2 and 19 wt%, with lower solidus temperatures of 645 °C and liquidus up to approximately 825 °C for low P and Ag compositions [12]. Newer filler metals may add further alloying additions; commercially available Vitrobraze™ VZ2255 (or Meta-Braze™ 077), based on Cu-Sn-Ni-P with a narrow melting range of 600 – 630 °C, was developed for use in CuproBraze® heat exchangers [5], where the aforementioned Cu-P and Cu-Ag-P filler metals possess too high a melting temperature to be suitable for joining the alloys used in the heat exchanger construction. The formation of the Cu_3P intermetallic compound [13] in the filler metals can be avoided by using the melt-spinning technique to produce amorphous thin foils [14,15], which is beneficial as the flexibility of the foil allows cutting to shape and greater gap width control [15]. With all such filler metals, however, joints may exhibit formation of Cu_3P post-braze, which can propagate cracks and thus compromise joint mechanical properties [15–18]. Furthermore, tin content, while further helping to reduce filler metal melting temperature without increased phosphorus content, can affect the wetting ability of the molten filler metal, leading to the requirement of a fluxing agent at approximately 7 wt% [19].

Due to their beneficial mechanical and corrosion properties, Cu-based filler metals have the potential to be used in a wider variety of applications, particularly for joining Cu and brasses used for more efficient heat exchange in electric vehicles (as compared to Al alloys used in conventional automobiles). Furthermore, Cu-based filler metals have properties potentially beneficial for the joining of materials with greatly different mechanical properties, such as dissimilar and sometimes bespoke metal-ceramic joints for use at elevated temperatures. To date, however, options are limited when selecting a copper-based filler metal with a low melting temperature while retaining higher operating temperature capability, particularly where significant Cu_3P content is present post-braze. This report details the design of three Cu-based filler metals, based around the commercial Meta-Braze™ 077 filler metal, aiming to address these limitations. The CALPHAD-based software Thermo-Calc was used first to investigate predicted phase abundance in such systems, and then to investigate compositional alterations that may improve high temperature performance through reducing brittle low-temperature Cu_3P phase abundance, and increasing melting range of Cu-rich solid solution phase. Three selected compositions were fabricated and used to braze pure copper as a test of this concept. The joint microstructure and properties are discussed.

2. Alloy design in thermo-calc

Commercially available filler metal Meta-Braze™ 077, based on the Cu-Ni-Sn-P system (composition Cu-7Ni-9.3Sn-6.3 P (in wt%)), was evaluated in Thermo-Calc (TC) as a baseline for comparison. The database used in the TC predictions was the SSOL4 database, which unlike other more specialised databases steels (TCFE databases) or Ni alloys (TCNI databases), allows for the inclusion of elements Sn and P in the prediction. All binaries except the Sn-P binary have been assessed in this database, though the only ternary system assessed is the Cu-Ni-Sn ternary system.

Fig. 1 shows the TC predicted equilibrium phase fraction as a function of temperature for the Meta-Braze™ 077 filler metal. Upon the start of solidification at approximately 730 °C, an FCC A1 solid solution (Cu-rich) is predicted to form, followed by formation of Ni_5P_2 intermetallic phase at approximately 675 °C. At slightly below 600 °C, eutectic solidification remaining liquid to form Cu_3P and further FCC A1 solid

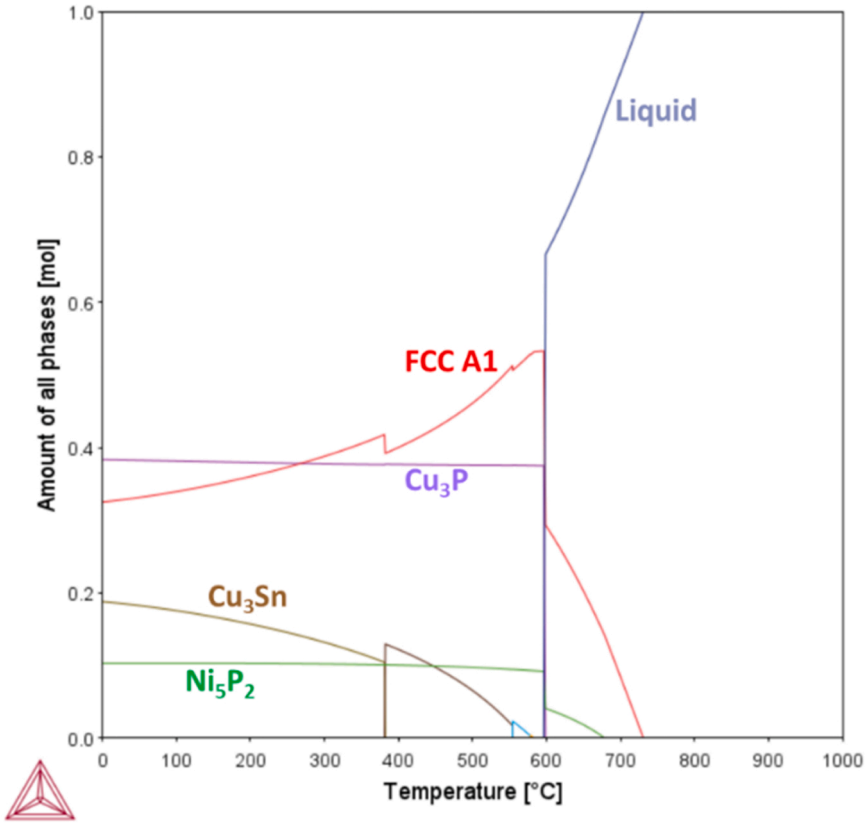

Fig. 1. TC equilibrium prediction (using SSOL4 database) of phase abundance as a function of temperature for the commercial Cu-7Ni-9.3Sn-6.3 P filler metal composition.

solution. Cu_3Sn is also predicted to form at lower temperatures, stable down to room temperature and coinciding with decreasing FCC A1 fraction, suggesting that the solid solution is saturated with Sn and leading to formation of the intermetallic phase. Meta-Braze™ 077 filler metal has a melting range of 600 – 630 °C; the discrepancy between this industry-quoted liquidus and the TC predicted liquidus, aside from the fact that TC predictions represent equilibrium conditions, may be explained by the eutectic temperature of approximately 600 °C, apparently captured by TC and in agreement with the quoted solidus value. In practical usage, sufficient liquid may be present at 630 °C so as to be used in brazing, hence the quoted melting range.

One approach to improve joint performance at elevated temperatures above 360 °C, while remaining within the same alloy system, would be to decrease the proportion of low temperature eutectic Cu_3P in the joint and increase the proportion of FCC Cu-rich solid solution, via compositional optimisation. A reduction in P content may achieve this, yet too great a reduction would also increase the initial melting temperature of the filler metal, potentially rendering it useless for application. Some reliance may be placed upon P diffusion away from the joint (comparatively fast as compared Sn or Ni) in order to further reduce final joint P content, and thus reduce final joint eutectic content. Likewise, Sn and Ni content can be altered in order to impart improved mechanical properties through solid solution strengthening (increasing Ni content), and to tailor the melting range to reduce softening at high temperature. Further balances must, however, be struck. Aside from microstructural and melting range concerns, too great a reduction in Sn and P may be expected to inhibit flow characteristics of the molten filler metal. Meanwhile, too much an increase in Ni content may increase the initial liquidus of the filler metal undesirably high for the application.

Based upon the composition of the Meta-Braze™ 077 filler metal, Fig. 2 shows the colour intensity chart of predicted molar fraction of FCC A1 solid solution at 590 °C (just below eutectic transformation), for varying Sn and P content (0–10 wt%) in a Cu-7Ni alloy. Compositions containing 5 wt% or less of P are predicted to possess a 0.6 molar fraction FCC A1 solid solution component, and hence likely contain a smaller eutectic component, as compared to that predicted for the commercial Meta-Braze™ 077 filler metal (it can also be inferred from Fig. 2 that the composition of the Meta-Braze™ 077 filler metal would be predicted to have a FCC A1 fraction of below 0.5). Meanwhile, considering a range of commercially employed Cu-P filler metals, P content is most commonly in excess of 5 wt%, possibly due to the beneficial self-fluxing effect of filler metals with such P contents, and so compositions containing P less than this were not considered. Therefore a composition (in wt%) of Cu-7Ni-4Sn-5 P was considered for a prospective alloy (Alloy 1 hereafter). Fig. 3 shows TC predictions of phase fraction as a function of temperature for this composition. Predicted room temperature phase fraction of Cu_3P eutectic phase is notably lower than was predicted for the Meta-Braze™ 077 composition, below 0.3 molar fraction, while FCC A1 fraction is approximately 0.55. Fraction of predicted Cu_3Sn is also much reduced, while predicted Ni_5Sn_2 fraction is unchanged. Predicted liquidus temperature of the FCC A1 phase is also notably increased, predicted at approximately 885 °C as compared to approximately 730 °C for the Meta-Braze™ 077 composition.

With limited scope for further reductions in P content, increased Ni content was considered for promoting FCC solid solution formation and improving high temperature strength, albeit at the cost of potentially higher melting temperature. Fig. 4 shows the colour intensity chart of predicted molar fraction of FCC A1 solid solution at 590 °C, for varying Sn and P content (0–10 wt%) in a Cu-10Ni alloy. The trends observed are largely the same as presented in Fig. 2 at slightly increased Sn contents. As such, a composition (in wt%) of Cu-10Ni-5Sn-5 P was considered as a second prospective alloy (Alloy 2 hereafter). Fig. 5 shows TC predictions of phase fraction as a function of temperature for this composition. As compared to Fig. 3, a still greater reduction in Cu_3P fraction at room temperature was predicted, while room temperature FCC A1 fraction was similar. Predicted room temperature fraction of Ni_5P_2 was increased due to increased Ni content. Liquidus temperature of the FCC A1 phase is slightly increased, predicted at approximately 890 °C.

In addition, a further alloy was considered with further reduced Sn content in order to suppress predicted Cu_3Sn phase. Sn may also be detrimental to ductility and increase the need for using a fluxing agent [19]. Meanwhile higher P can reduce need for fluxing agent and may

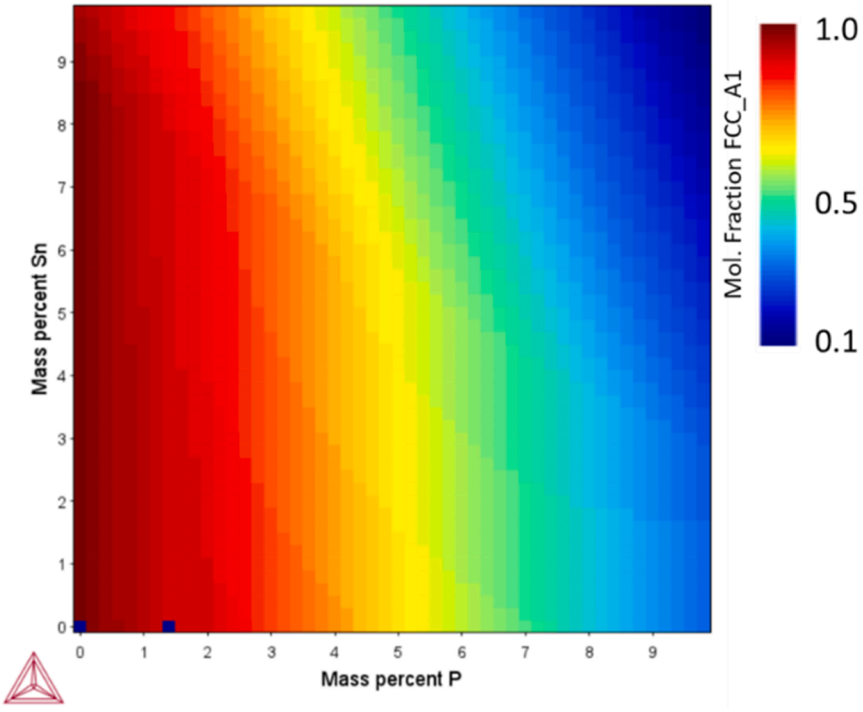

Fig. 2. TC colour intensity chart, showing predicted fraction of FCC A1 phase at 590 °C for a range (0–10 wt%) of Sn and P contents in a Cu-7Ni system. Dark red represents compositions with a FCC A1 fraction of 1.0, while dark blue represents a fraction of 0.1 or less.

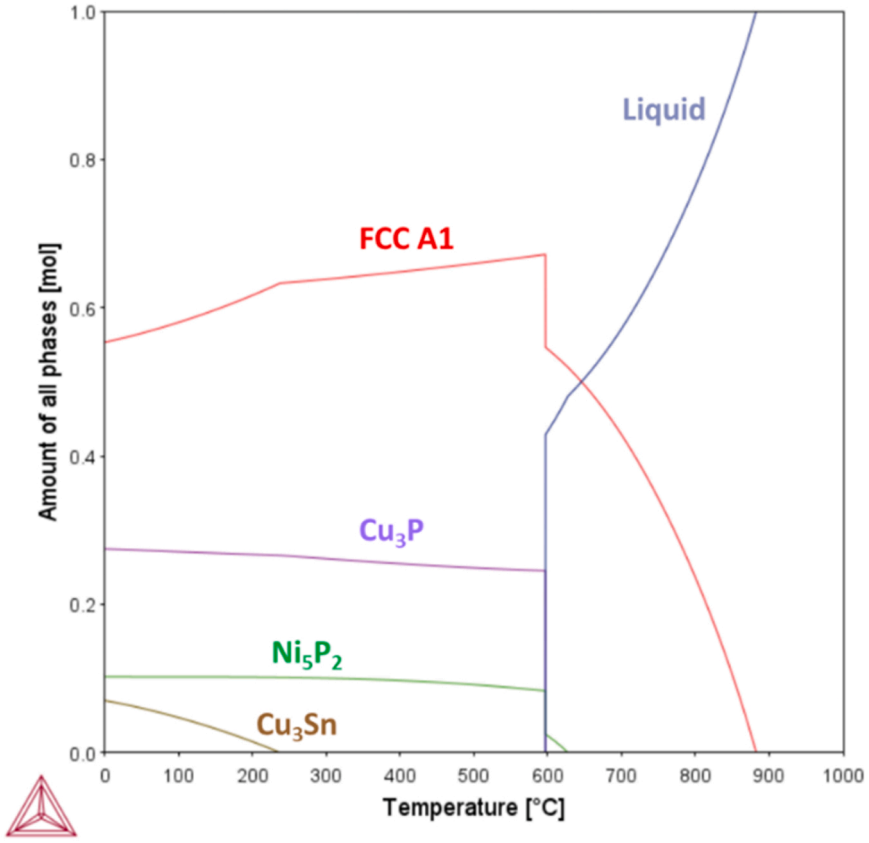

Fig. 3. TC predictions of phase fraction as a function of temperature for the Cu-7Ni-4Sn-5 P (wt%) composition.

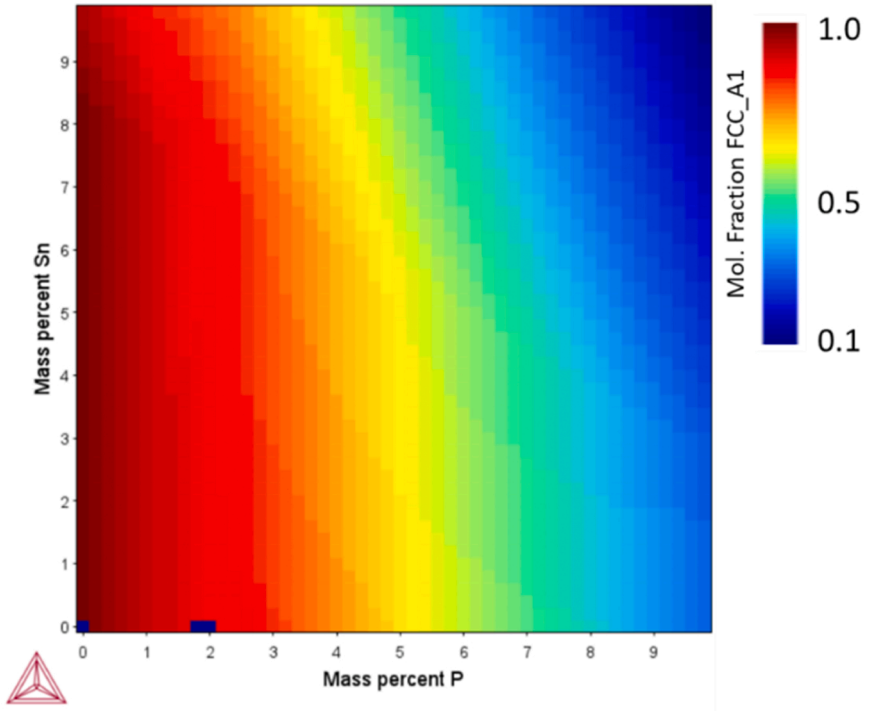

Fig. 4. TC colour intensity chart, showing predicted fraction of FCC A1 phase at 590 °C for a range (0–10 wt%) of Sn and P contents in a Cu-10Ni system. Dark red represents compositions with a FCC A1 fraction of 1.0, while dark blue represents a fraction of 0.1 or less.

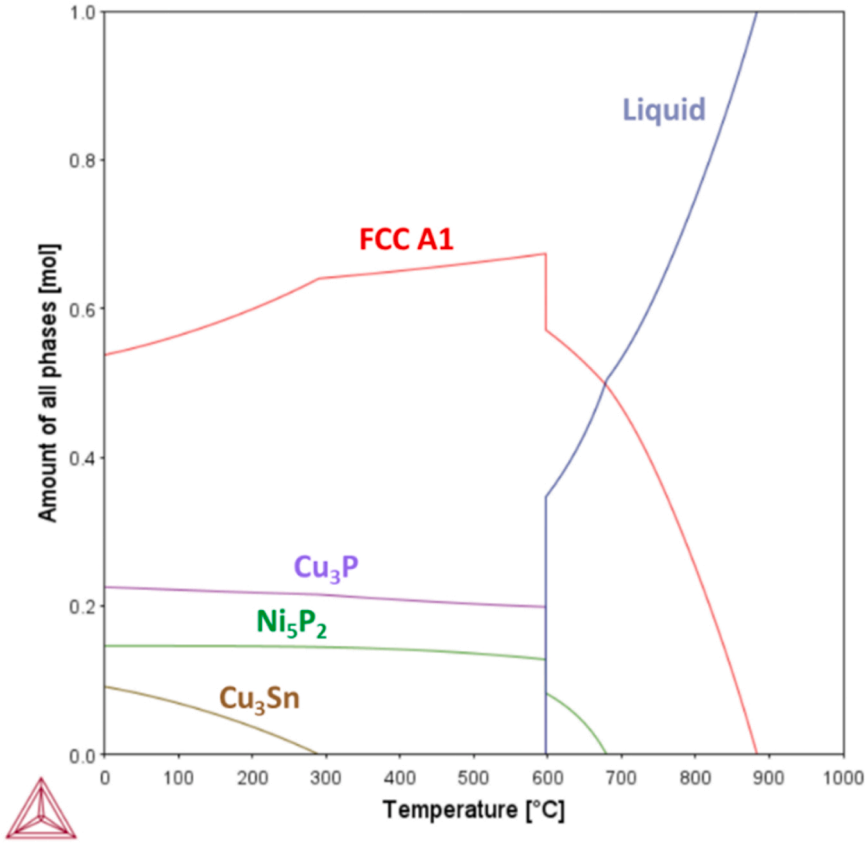

Fig. 5. TC predictions of phase fraction as a function of temperature for the Cu-10Ni-5Sn-5 P (wt%) composition.

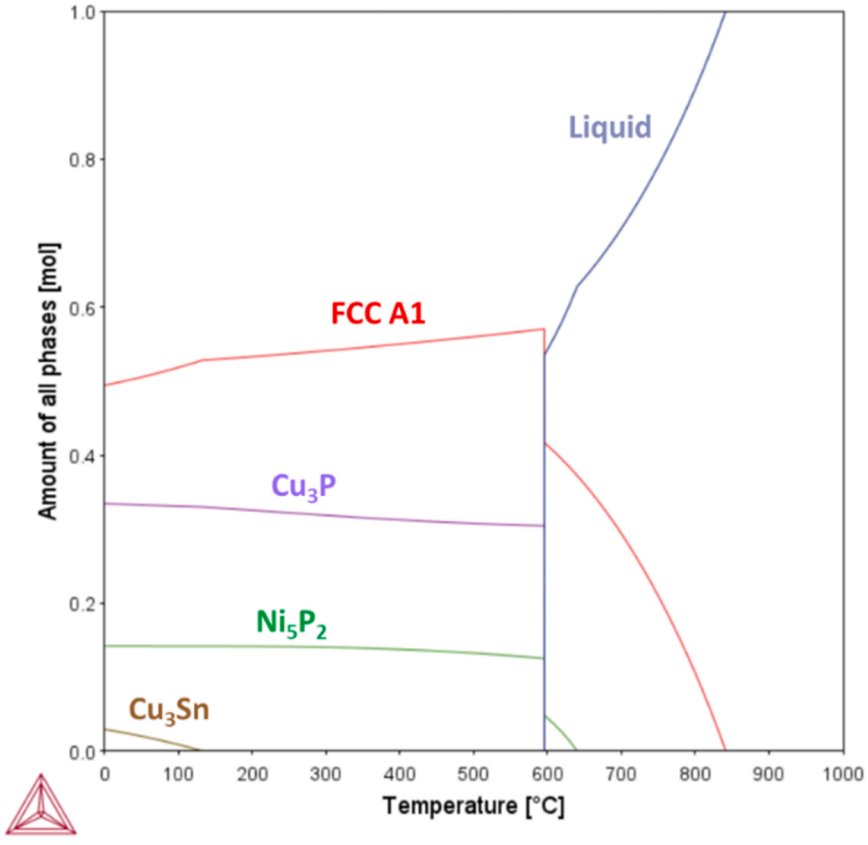

Fig. 6. TC predictions of phase fraction as a function of temperature for the Cu-10Ni-2Sn-6.5 P (wt%) composition.

ensure sufficient melting while allowing reduced Sn. The composition (in wt%) of the third alloy was Cu-10Ni-2Sn-6.5 P (Alloy 3 hereafter). Fig. 6 shows TC predictions of phase fraction as a function of temperature for this composition. Room temperature fraction of Cu_3P is somewhat increased compared to Figs. 3 and 5, at approximately 0.33, while Ni_5Sn_2 fraction comparable to that in Fig. 5. Predicted Cu_3Sn phase fraction is greatly reduced, though predicted FCC A1 fraction is the lowest of the three proposed compositions.(Table 1).

3. Experimental methods

3.1. Alloy fabrication

Alloys 1, 2 and 3 were fabricated via vacuum arc-melting (Arcast Arc-200) from elemental Cu (foil), Ni (foil) and Sn (wire), all of purity of at least 99.9%. In addition, pre-alloyed Cu-P brazing rod (commercial name Meta-Braze™ 182, supplied by VBC Group, Loughborough, UK), of composition (in at%) Cu-14.8 P, was used to introduce P to the alloys. The arc-melting procedure involved twice inducing a vacuum of less than 5×10^{-2} mbar (5×10^{-3} kPa) followed by backfilling with Ar to a pressure of − 50 kPa, before inducing a final vacuum of below 4×10^{-5} mbar (4×10^{-6} kPa), with Ar then backfilled to a pressure of approximately − 30 kPa. An operating current of 400 A was applied to a W electrode, and 30 g ingots were produced which were flipped and re-melted five times to improve homogeneity. As-cast ingots were sectioned for characterisation (details below), with approximately 15–20 g retained for foil production via melt-spinning (Arcast SC 100). Material was placed in a boron nitride crucible with 20 × 1 mm slit for melt ejection. The crucible was placed such that the melt drop height on to the water-cooled Cu wheel was approximately 7 mm, and the wheel rotation speed was set at approximately 30 ms^{-1}. An induction coil was used to melt the material, with power of approximately 1.7 kW supplied until a measured crucible temperature of approximately 850 °C was reached. Ejection of the melt was aided by the introduction of approximately 30 in Hg pressure of Ar.

Manual torch (oxyacetylene) brazing trials of alloys 1, 2, 3 and commercial Meta-Braze™ 077 were conducted on tokens of pure Cu (99.95%) with dimensions 25×25×3 mm, arranged in a sandwich joint configuration. Cu tokens were ground with p1200 SiC paper prior to bathing in acetone, with melt-spun placed in between the tokens. Alloys 1, 2 and 3 foils were of average thickness between 80 and 120 μm, and commercial Meta-Braze™ 077 foil was of average thickness 30 – 50 μm. To achieve a more similar initial thickness of filler metal prior to brazing, the Meta-Braze™ 077 foil was double-layered. The torch flame was then applied to the joint maintaining a distance of approximately 100 mm to ensure even heating. Heat was applied to the joints until such a point that further heating may risk melting of Cu tokens (3 min for Meta-Braze™ 077, 2.5 min for Alloy 1 and Alloy 2, and 2 min for Alloy 3).

3.2. Characterisation techniques

The as-cast microstructures of alloys 1, 2 and 3 were observed via scanning electron microscopy (SEM) (FEI Inspect F50) in backscattered electron (BSE) mode, with elemental distribution analysed via energy dispersive X-ray spectroscopy (EDS) maps and point scans. Phases were further identified via X-ray diffraction (XRD)(Bruker D2 Phaser). Vickers microhardness (Struers Durascan) was measured for each alloy (average of 10 measurements). Melting range of melt-spun foils of alloys 1, 2 and 3, as well as for commercial Meta-Braze™ 077, was inferred from DSC measurements (Netzsch 404 F1 Pegasus), performed in Ar atmosphere with heating rates of 20 °C min^{-1}, and sample masses were approximately 10 mg. Post-brazing, joints were sectioned and characterised via SEM, EDS, and Vickers microhardness as above.

Table 1
Nominal compositions in wt% (at%) of commercial Meta-Braze™ 077, and selected compositions of interest following TC design process.

	Nominal composition in wt% (at%)			
Alloy	**Cu**	**Ni**	**Sn**	**P**
Meta-Braze™ 077	77.4 (75.2)	7 (7.4)	9.3 (4.8)	6.3 (12.6)
1	84 (80.8)	7 (7.3)	4 (2.1)	5 (9.9)
2	80 (77.1)	10 (10.4)	5 (2.6)	5 (9.9)
3	81.5 (76.4)	10 (10.1)	2 (1.0)	6.5 (12.5)

4. Results & discussion

4.1. As-cast alloy characterisation

Fig. 7 shows the BSE image for Alloy 1 along with EDS maps showing elemental distribution between phases. Cu-rich dendrites were observed, changing to Cu-Sn-rich around the dendrite edges. Meanwhile, Ni and P are concentrated in the interdendritic spaces, with enhanced Ni concentration coinciding with the darkest contrast intermetallic phase, where Cu is most lean. The dark grey interdendritic phase is richer in Cu, as well as P. Fig. 8 shows a higher magnification BSE image with four distinct phases labelled, along with EDS point scan measurements (average of five measurements per phase). Point scan measurements confirmed the presence of Cu solid solution in the dendrite structures, richer in Sn towards the edges, with interdendritic Cu_3P intermetallic, possibly formed from eutectic solidification of remaining melt, as well as $Ni(Cu)_2P$ intermetallic.(Table 2).

As can be seen in Fig. 9, Alloy 2 exhibited a similar microstructure to Alloy 1, but with increased proportion of eutectic structure mostly around the Cu-Sn dendrites. The proportion of $Ni(Cu)_2P$ intermetallic phase was also increased as compared to Alloy 1. EDS point scans at higher magnification, as shown in Fig. 10, reveal that the phase compositions are largely similar to those seen in Alloy 1. Fig. 11 shows a somewhat different microstructure in Alloy 3 as compare to Alloys 2 and 3, with the main difference being the more elongated and continuous morphology of Cu-Sn dendrites contrasted with the more globular and discontinuous morphology in Alloys 1 and 2. Meanwhile, EDS point scans (Fig. 12) confirmed the phases to still be of similar compositions to those measured in Alloys 1 and 2. While Sn was observed to be still concentrated around the dendrite edges, its abundance was decreased, in line with the reduced Sn content of Alloy 3. Furthermore, the proportion of Cu observed in the $Ni(Cu)_2P$ intermetallic phase was observed to increase across Alloys 1–3 (increasing from 4.4 to 8.6 at% from Alloy 1 to Alloy 3).(Table 3).

Microstructural analysis of all three fabricated alloys in the as-cast state revealed microstructures largely in agreement with TC predictions in terms of phases present, namely Cu-rich solid solution, and eutectic Cu_3P and Ni_2P phases. Also observed surrounding the dendrites of Cu-rich solid solution were regions of higher Sn content, which was not captured by the TC predictions. The formation of this microstructure therefore likely resulted from the partitioning of Sn and particularly P from the solidifying Cu-rich dendrite cores (partition coefficients of Sn and P in Cu are approximately 0.57 and 0.22 respectively, according to the binary phase diagrams), enriching the surrounding melt with Sn, which then solidified upon cooling, followed by final eutectic transformation of remaining P-rich melt to form Cu-solid solution and Cu_3P:

$$\text{Cu-rich solid solution} \rightarrow \text{Cu-Sn-rich solid solution} \rightarrow \text{Cu solid solution} + Cu_3P$$

This Sn-enhanced region was however suppressed in Alloy 3, the most Sn-lean of the developed alloys, and Cu-rich solid solution dendrites appeared to be more continuous rather than globular in morphology, perhaps due to the lower Sn content. Meanwhile, all alloys exhibited irregular morphology Ni_2P phase, but with increasing amounts of Cu in solution from Alloy 1–3. Likewise, Cu_3P phase was observed in all three alloys, with small amounts of Ni in solution again

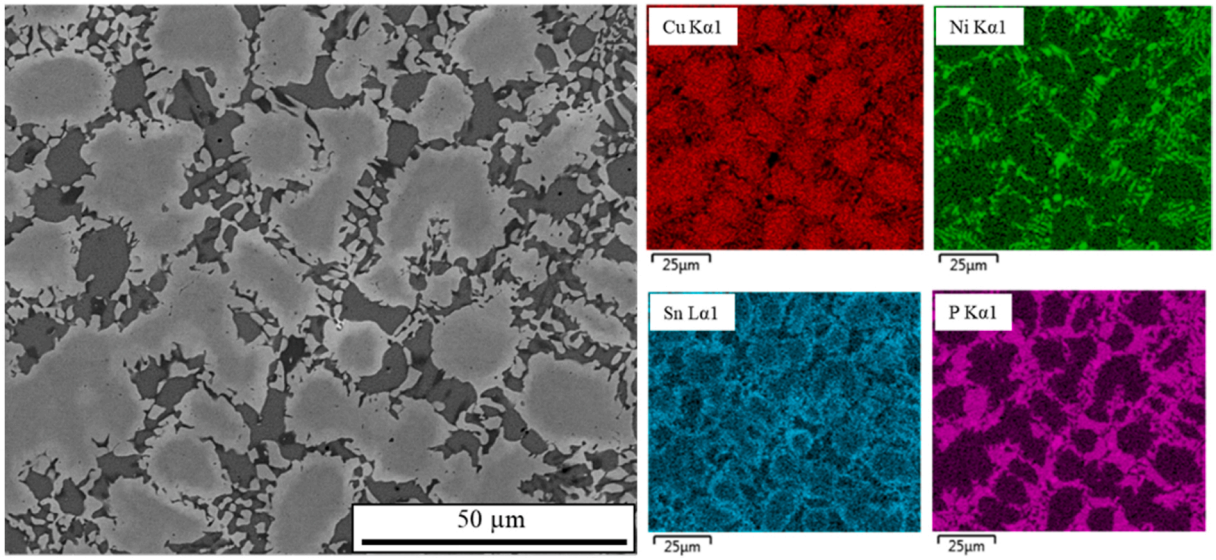

Fig. 7. SEM BSE image of Alloy 1 along with EDS maps showing elemental distribution between phases.

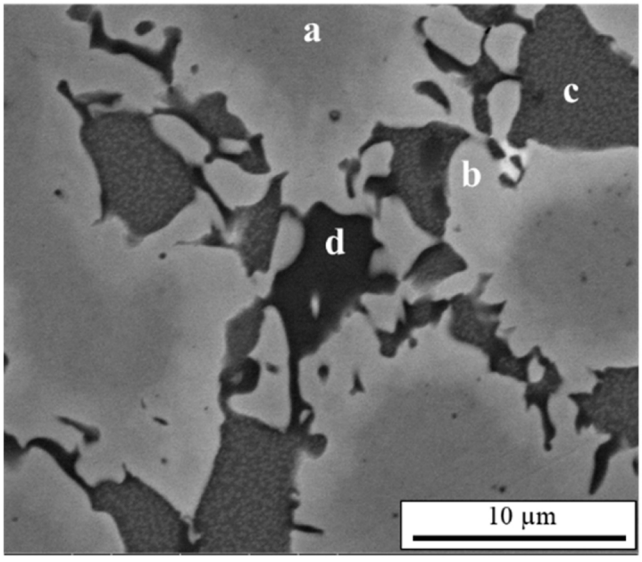

Fig. 8. High magnification SEM BSE image of Alloy 1 with four identified phases labelled, along with EDS point scan measurements (average of five measurement for each phase).

Table 2
EDS point scan measurements (at%) made at representative locations indicated in Fig. 8 (average of five measurements), along with possible phase at location.

Area	Cu	Ni	Sn	P	Phase
a	96.7	1.2	0.9	1.2	Cu solid solution
b	90.7	1.1	6.9	1.3	Cu solid solution
c	73.8	1.2	0.9	24.9	Cu_3P
d	4.4	62.4	0.1	33.1	$Ni(Cu)_2P$

increasing somewhat from Alloys 1–3 (this result may however fall within the margin of error expected for EDS point analysis).

SEM and EDS analysis was complimented with X-ray diffraction (XRD) phase analysis. Fig. 13 shows diffraction spectra for Alloys 1, 2 and 3, with identified phase peaks labelled. While distinct peaks for the Cu-rich and Cu-Sn-rich were not observed (due to the Sn still remaining in solution even at higher concentrations), peaks for Cu-solid solution, Cu_3P and Ni_2P were identified, corresponding well to SEM and EDS observations.

In order to infer potential effects on the mechanical properties of the as-cast states of Alloys 1, 2 and 3, Vickers microhardness was measured (Fig. 14). While microhardness differences were small, Alloy 2 exhibited the highest microhardness of the three, and Alloy 3 the lowest. This is possibly explained by Alloy 2 having slightly more alloying additions (in total at%), as well as an apparently increased $Ni(Cu)_2P$ content, but also by Alloy 3 having the lowest Sn content and possibly greater proportion of Cu-rich solid solution. It is also noted that the measurement error, derived from standard deviation of 10 measurements, is greater for Alloys 1 and 2 than for Alloy 3. This is possibly due to the greater proportion of interdendritic regions in Alloys 1 and 2, producing greater variance due to the difference in hardness between the Cu_3P and Cu-rich/Cu-Sn-rich phases.

DSC heating and cooling curves (second cycle) up to approximately 1000 °C of amorphous foil Meta-Braze™ 077 and melt-spun foils of Alloys 1, 2 and 3 are shown in Fig. 15. In the heating curves, peaks for all four foils were observed at approximately 600 °C (Meta-Braze™ 077) and 620 °C (Alloys 1, 2 and 3). This is in close agreement with the industrially-quoted melting range of the Meta-Braze™ 077 (600–625 °C), though this is presumably for the amorphous state in which the foil is supplied. In the cooling curve presented in Fig. 15, the foils have all undergone melting, and so it is expected that any amorphous component from the melt-spinning is no longer present. Likely, the lowest melting point phase present (inferred from the as-cast states of alloys 1, 2 and 3) is expected to be the Cu_3P phase, melting at 710 °C according to the Cu-P binary phase diagram. These peaks therefore possibly correspond to the melting of this phase, with discrepancy in the melting point possibly due to differing compositions of the phase in each alloy (from EDS scans shown in Table 4, the Cu_3P phase had a small Ni and Sn content). No further events were captured by the heating curve, however during cooling Alloys 1 and 3 displayed an additional peak at 800 °C and 825 °C respectively, and at approximately 650 °C for the Meta-Braze™ 077 foil. In each case, it was deemed unlikely to correspond to melting of the Cu-rich solid solution, and instead (for the latter former peaks) may correspond to the Ni-Ni_3P eutectic temperature (891 °C), though why this same peak does not appear in the cooling curve for Alloy 2 is unclear. Furthermore, Ni_3P phase was not observed in EDS measurements in the Alloys developed in this study. It is also unclear what the latter peak is here, and analysis of an as-cast state of the Meta-Braze™ 077 composition may be needed to interrogate this

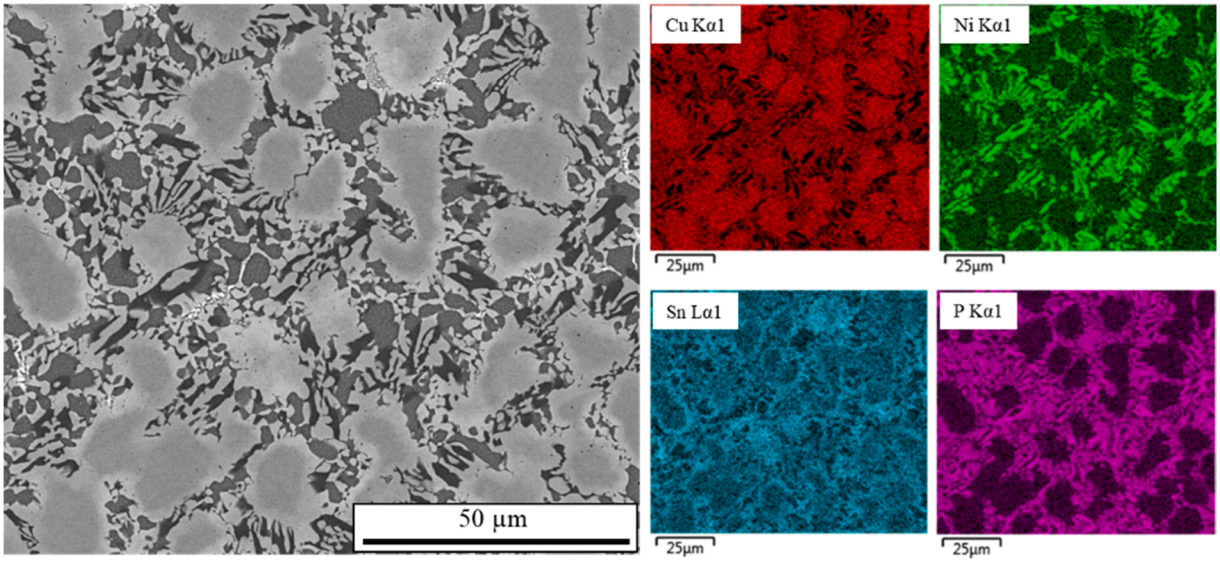

Fig. 9. SEM BSE image of Alloy 2 along with EDS maps showing elemental distribution between phases.

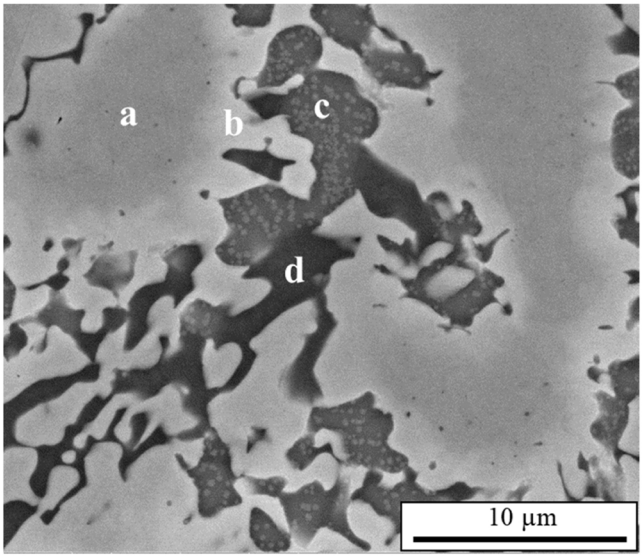

Fig. 10. High magnification SEM BSE image of Alloy 2 with four identified phases labelled, along with EDS point scan measurements (average of five measurement for each phase).

further.

4.2. Brazed joints characterisation

Fig. 16 shows an SEM BSE image of a representative section of the joint using the commercial Meta-Braze™ 077 filler metal, along with EDS maps indicating elemental distribution. The joint width was observed to have good consistency, at approximately 80 – 90 μm. The joint microstructure displays multiple distinct phases; Cu-rich dendrites of irregular size and morphology (marked 1); Cu-Sn-rich solid solution towards the dendrite edges (marked 2); fine eutectic Cu_3P + Cu solid solution (marked 3) representing perhaps a majority of the joint; larger irregular morphology Cu_3P phase; and sporadic $Ni(Cu)_2P$ phase of below approximately 10 μm in size (marked 5, inferred by the EDS maps). (Table 5).

Fig. 17 shows an SEM BSE image of a representative section of the joint using Alloy 1 as the filler metal, in addition to EDS maps indicating elemental distribution. The joint width was slightly greater than for the joint using Meta-Braze™ 077, at approximately 100 μm, and similar phases were observed. However, the large irregular morphology Cu_3P phase seen in Fig. 16 (marked 4) was notably absent in Fig. 17, and the eutectic Cu_3P + Cu solid solution regions exhibited increased coarseness as compared to the finer lamellar structure seen in Fig. 16. Also, the Cu-rich solid solution dendrites were apparently increased in size and represented a larger proportion of the joint region. It may also be inferred from Table 2 that the observed $Ni(Cu)_2P$ phase seen in the as-cast Alloy 1 has increased in Cu post-braze.

Fig. 18 shows SEM BSE image and EDS maps for the joint using Alloy 2 as filler metal. Immediately noticeable is the increased joint width, at approximately 130 μm, resulting from the greater initial foil thickness. Again, similar phases were observed, and Cu-rich solid solution dendrites represented the majority of the joint. However, interdendritic regions were characterised by coarser Cu_3P and smaller regions of Cu-Sn rich solid solution, as opposed to the finer eutectic Cu_3P + Cu solid solution regions seen in Figs. 16 and 17. Furthermore, the concentration of the intermetallic $Ni(Cu)_3P$ phase appeared to be increased.

Lastly, Figure 29 shows SEM BSE image and EDS maps for the joint using Alloy 3 as filler metal. The joint width was again significantly greater here, at approximately 200 μm, due to initial foil thickness. This, and the limited time held at temperature, may be expected to inhibit the isothermal solidification of the melt (which in known to be sensitive to time, temperature and joint chemistry), But despite this, the joint appeared to predominantly consist of more continuous Cu-rich solid solution dendrites with much sparser pockets of Cu-Sn rich solid solution at dendrite edges as compared to the previous joints. In addition, the interdendritic regions were characterised by occasional eutectic structure Cu_3P + Cu solid solution, and $Ni(Cu)_3P$. Table 2 shows EDS point scan measurements of different regions labelled in Figs. 16–19, except where the feature is too small to obtain accurate measurement. Utilising the contrast between phases in Figs. 16–19, ImageJ software was used to determine approximate area fraction of solid solution phase in each joint, as shown in Fig. 20.

Upon trialling of Alloys 1 − 3 and Meta-Braze™ 077 in the brazing of pure Cu, the main difference immediately observed was the difference in flow characteristics, evidenced by an inability to effectively wet and spread into the gap between Cu tokens by Alloys 1 – 3, whereas this was accomplished much more readily for the commercial Meta-Braze™ 077. As such, joints using Alloys 1 – 3 remained greater in width despite melting of the filler metal, whereas filler metals good at wetting may be

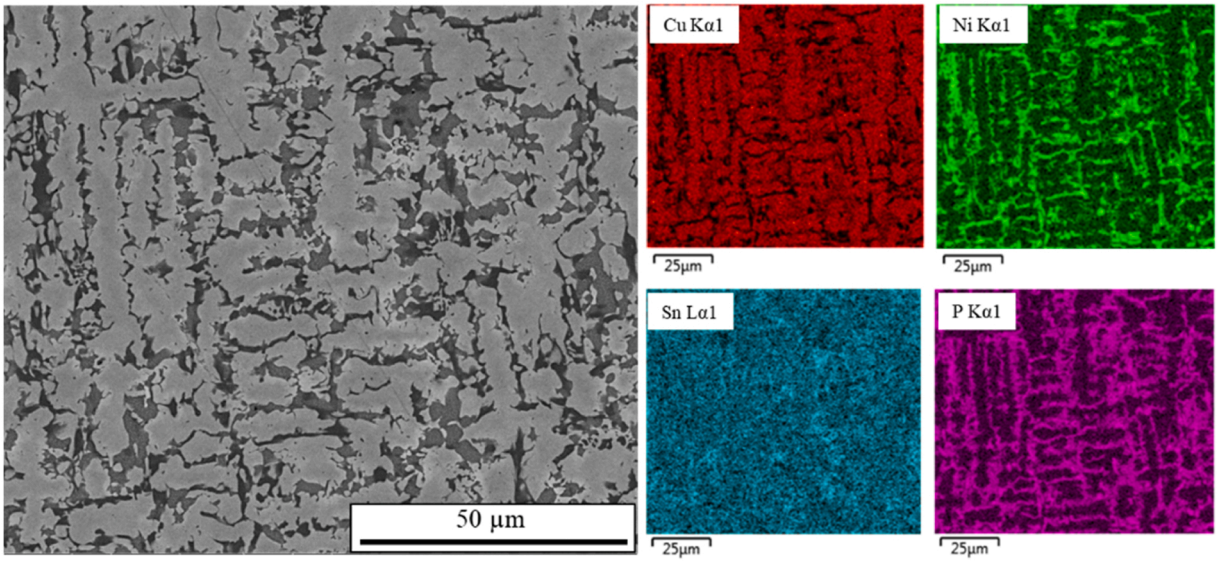

Fig. 11. SEM BSE image of Alloy 3 along with EDS maps showing elemental distribution between phases.

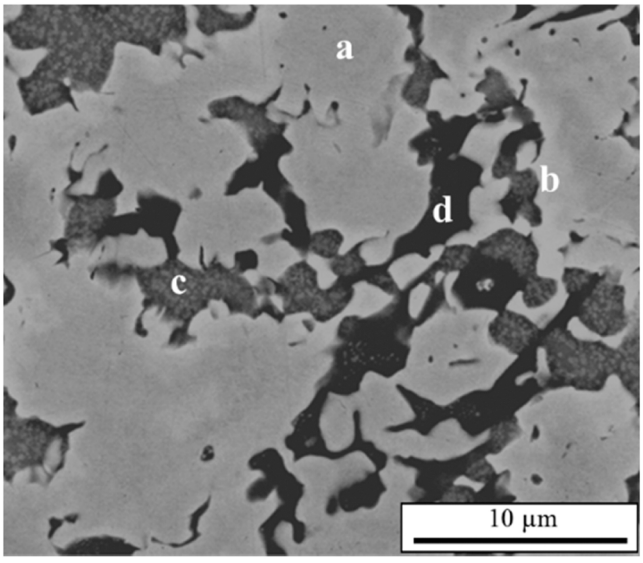

Fig. 12. High magnification SEM BSE image of Alloy 3 with four identified phases labelled, along with EDS point scan measurements (average of five measurement for each phase).

Table 3
EDS point scan measurements (at%) made at representative locations indicated in Fig. 10 (average of five measurements), along with possible phase at location.

Area	Cu	Ni	Sn	P	Phase
a	96.1	2.0	1.1	0.8	Cu solid solution
b	87.9	2.7	6.5	2.9	Cu solid solution
c	73.6	1.5	0.3	24.5	Cu_3P
d	6.0	61.2	0.2	32.6	$Ni(Cu)_2P$

expected to spread throughout the joint and allow the joint gap to decrease due to the weight of the upper base metal piece. The reasons for this poor flow performance as compared to Meta-Braze™ 077 may therefore be due to the compositions of the developed filler metals, containing both less Sn and P (Alloys 1 and 2 contain a reduced amount of Sn as compared to the commercial Meta-Braze™ 077, as well as a small reduction in P, while Alloy 3 had greater reduction in Sn concentration but a slight increase in P). Indeed, slight deviations in P content away from eutectic composition can rapidly increase melting range [13] and perhaps inhibit flow this way.

The microstructures exhibited by the joints using Meta-Braze™ 077, and Alloys 1 – 3 all show comparable features in terms of phases but with observed differences in their abundance. When Meta-Braze™ 077 filler metal was used, the joint exhibited large regions of intermetallic phases, and the fraction of Cu-rich solid solution was the lowest of all joints, at approximately 0.61. A particular feature was the large irregular morphology Cu_3P phase (such as marked 4 on Fig. 16), which was not observed for other joints. Much of the joint in fact consisted of fine eutectic structure containing much of the Cu-rich solid solution, with only sporadic regions of larger Cu-rich solid solution dendrites (such as marked 1 in Fig. 16). The morphology of the interface with the pure Cu base metal is also noteworthy, being observably wavy with columnar protrusions of apparently Cu-Sn rich solid solution. The lighter contrast of this interface region suggests Sn enrichment in a region of between 10 and 25 µm on average. These are of greater size at the bottom of the joint micrograph displayed in Fig. 16, extending up to approximately 40 µm towards the joint centre, compared with approximately 20 µm for the protrusions at the top of the joint. This may in fact be as a result of uneven heat and cooling of the joint, caused by application of heat to predominantly one side of the joint, with the side experiencing elevated temperatures for longer times exhibiting increased isothermal solidification of the solid solution dendrites. When Alloy 2 was used as filler metal, the fraction of Cu-rich solid solution was found to be only slightly increased, at approximately 0.66. The fine eutectic structure observed in the Meta-Braze™ 077 joint was absent in this joint. A combination of increased Ni content, which possibly resulted in an increase Ni-P intermetallics - particularly given the greater mixing enthalpy of P and Ni (-34.5 kJ mol^{-1}) compared to P and Cu (-17.5 kJ mol^{-1}) [20] - and an increase in joint width due to the initial melt-spun foil thickness, likely contributed to this. Despite this, an increase in Cu-rich solid solution dendrites was observed as compared to the joint using Meta-Braze™ 077 as filler metal. The interface with pure Cu base metal was also less wave-like in morphology, with protrusions noticeably less prominent and generally less than 10 µm in length, with no apparent difference between each side of the joint. With reduction of joint width in this case, it may be expected that increased diffusion may help to reduce the content of P in the joint region, and solid solution dendrites may coalesce and increase in fraction.

The joints using Alloys 1 and 3 by contrast exhibited features that

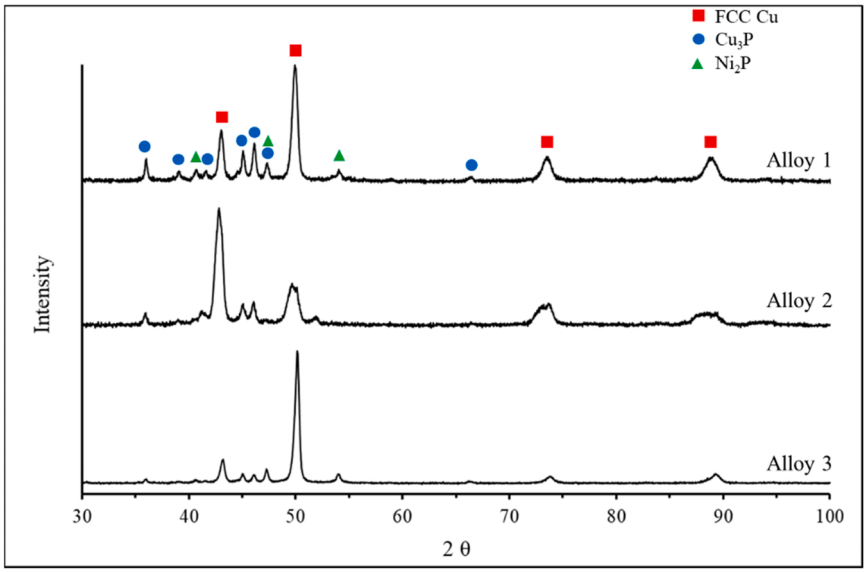

Fig. 13. XRD spectra of Alloys 1, 2 and 3, with identified peaks labelled for FCC Cu (corresponding to C-rich and Cu-Sn-rich solid solutions) and Cu_3P and Ni_2P intermetallic phases.

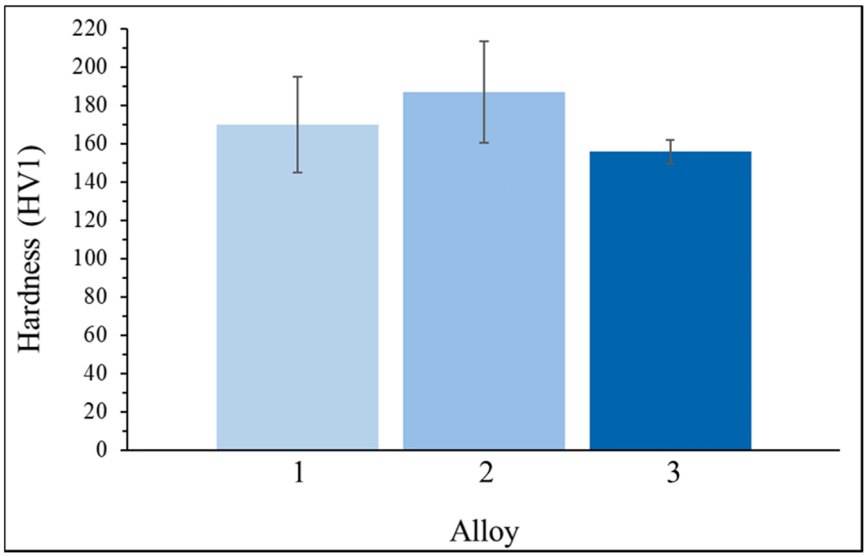

Fig. 14. Vickers microhardness measurements (average of 10 measurements) for as-cast Alloys 1, 2 and 3. Error bar derived from standard deviation of 10 measurements.

may be beneficial for joint strength. The joint width where Alloy 1 was used as filler metal was the narrowest of the joints using the developed filler metal alloys, at approximately 100 μm. The Sn-enhanced interface with pure Cu base metal, while wave-like as in the case of Meta-Braze™ 077, exhibited smaller solid solution protrusions. Cu-rich solid solution dendrites within the joint region were larger and represented an approximate fraction of 0.78, and the interdendritic region consisted of mostly eutectic structure, albeit coarser than that in the joint using Meta-Braze™ 077 filler metal. The Cu_3P intermetallic phase was therefore distributed in these structures rather than in the larger irregular morphology as seen in Fig. 16. The joint using Alloy 3 as filler metal bore many similarities, although it was the widest of the produced joints. As in the case where Alloy 1 was the filler metal, a wave-like interface was observed but with protrusions shorter than 20 μm on average, and the Sn-enhanced region was narrow at generally 10 μm or less. Sn-enhanced regions at the edges of the Cu-rich solid solution dendrites was also suppressed as was the case for the as-cast Alloy 3, consistent with the low Sn content of Alloy 3. The fraction of Cu-rich solid solution within the joint was also similar to the joint using Alloy 1, at approximately 0.77, and given the width of the joint it is conceivable that with a narrower joint this fraction may increase due to increased diffusion-induced isothermal solidification. The interdendritic regions consisted of sporadic pockets of coarse eutectic structure, in addition to the Ni $(Cu)_3P$ intermetallic phase.

The nature of the base metal interfaces of the above joints is likely to be controlled by joint width and Sn content. With a slightly positive (7 kJ mol^{-1}) mixing enthalpy of the Cu-Sn binary pair, and good solubility of Sn in Cu according to the binary phase diagram, the Sn content of the joints is found in solution rather than in intermetallic phases. The composition of Meta-Braze™ 077, however, has a comparatively high Sn:Cu ratio (approximately 0.12) of the four filler metals, and so the solution within the joints may be saturated at lower temperatures below 450 °C, and rejected Sn may instead form solution with dissolved Cu base metal in the vicinity of the base metal and forming the observed

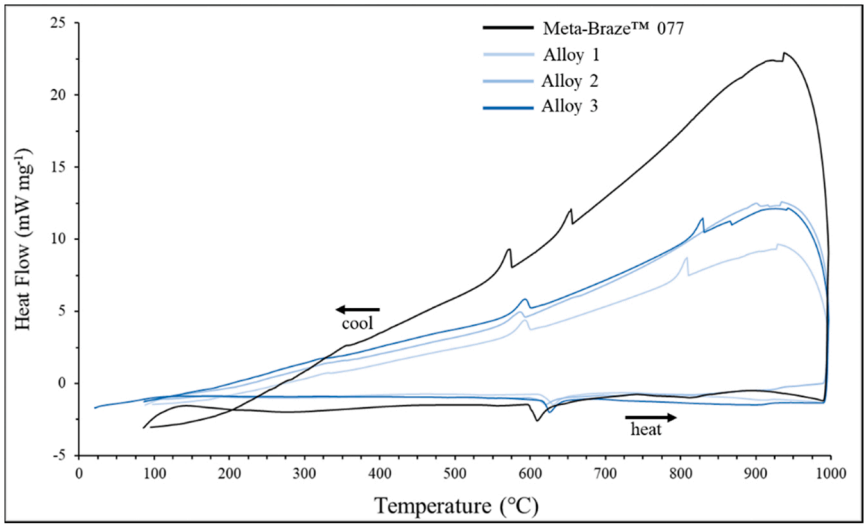

Fig. 15. Second-cycle DSC heating and cooling curves of commercial filler metal Meta-Braze™ 077 and developed melt-spun Alloys 1, 2 and 3.

Table 4
EDS point scan measurements (at%) made at representative locations indicated in Fig. 12 (average of five measurements), along with possible phase at location.

Area	Cu	Ni	Sn	P	Phase
a	95.9	1.4	1.2	1.5	Cu solid solution
b	92.0	1.7	2.6	3.7	Cu solid solution
c	72.2	3.4	0.1	24.3	Cu_3P
d	8.6	59.5	0.1	31.7	$Ni(Cu)_2P$

dendritic solid solution protrusions. The small joint width likely aided in Sn transport in this scenario. The Alloy 1 composition has a comparatively low Sn:Cu ratio (approximately 0.05), and so this phenomenon at the interface is less prominent, but again aided by the relatively small joint width. The Alloy 2 composition has a slightly higher relative Sn abundance (Sn:Cu ratio of 0.06), but increased gap size may have limited the Sn transport to the interface resulting in less prominent Sn-enriched protrusions. The Alloy 3 composition had the lowest relative Sn abundance (Sn:Cu ratio of 0.02) and the largest joint width, yet displays some interfacial Sn enrichment and more prominent protrusions than when Alloy 2 was the filler metal. It is possible therefore that the P content (highest in Alloy 3) plays some role in dissolving more of the base metal during the brazing process and aiding the formation of these features.

As discussed above, the width of a brazed joint plays a critical role in the microstructural evolution during brazing, and hence on the mechanical properties. For this reason, in order to allow comparison brazed joints should use as similar a filler metal thickness between all joints as possible. In the present study, it was impractical to attempt to obtain developed filler metal foils of the same thickness as each other and of the provided Meta-Braze™ 077, and so shear or tensile mechanical testing was not performed on the brazed joints. Nonetheless, likely trends in mechanical properties may be inferred, based on microstructural examination and on Vickers mircohardness profiles across the joints. Fig. 21 shows Vickers microhardness (HV0.05) profiles across joints brazed using each filler metal. As is typical with brazed joints containing regions of intermetallic phases and solid solution strengthening, microhardness was found to be increased within the joint, with the width of the increased region corresponding to the joint widths observed in Figs. 16 – 19. Joints using Meta-Braze™ 077 and Alloy 2 as filler metals exhibited the highest microhardness values in the joint regions, but for all joints the measured microhardness was maximum when the indentation was in the vicinity of intermetallic phases and eutectic regions, lower in the vicinity of the Cu-rich solid solution dendrites, and minimum in the pure Cu base metal. The microhardness profiles thus tend to be in agreement with Fig. 20, where joints using Alloy 1 and Alloy 3 as filler metal exhibited the highest fraction of Cu-rich solid solution phase. A flatter microhardness profile across a brazed joint may be an indication of greater homogeneity of ductility across the joint, which in most applications would be considered beneficial from a

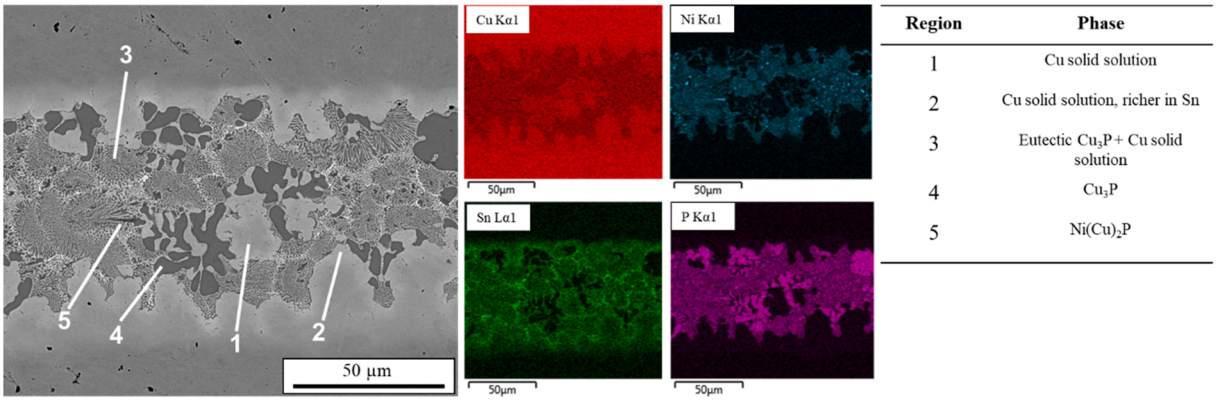

Region	Phase
1	Cu solid solution
2	Cu solid solution, richer in Sn
3	Eutectic Cu_3P + Cu solid solution
4	Cu_3P
5	$Ni(Cu)_2P$

Fig. 16. SEM (BSE) image of Cu tokens joined using commercial Meta-Braze™ 077 filler metal, along with EDS maps showing distribution of Cu, Ni, Sn, and P in the joint microstructure.

Table 5
EDS point scan measurements (at%) of different regions labelled when brazing Cu with Meta-Braze™ 077 (Fig. 16) and melt-spun Alloys 1, 2 and 3 (Figs. 17–19).

Filler metal	Figure	Region	Cu	Ni	Sn	P
Meta-Braze™ 077	17	1	94.9	0.7	3.0	1.3
		2	91.0	1.3	6.5	1.2
		3	*Feature too small*			
		4	73.4	0.9	0.1	24.0
		5	*Feature too small*			
Alloy 1	18	1	96.8	0.9	1.2	1.2
		2	93.5	0.9	4.5	1.1
		3	72.4	2.6	0.1	24.2
		4	7.6	60.3	0.1	32.0
Alloy 2	19	1	96.1	1.2	2.0	0.7
		2	93.1	0.7	5.2	1.0
		3	73.6	1.5	0.1	24.8
		4	27.7	47.7	-	24.7
Alloy 3	20	1	97.3	1.3	0.6	0.8
		2	74.4	1.0	0.1	24.7
		3	28.9	46.5	-	24.7

mechanical property standpoint, and so from this view Alloys 1 and Alloy 3 may be considered the most promising of the developed filler metals.

5. Conclusions

The main conclusions of this work can be summarised as follows:

- TC was used to design alloy compositions likely to possess a reduced content of brittle low-temperature phases such as Cu_3P, thus promoting a greater proportion of Cu-rich solid solution. In Alloy 1 this was achieved by reducing Sn and slightly reducing P content; in Alloy 2 this was achieved by reducing Sn and slightly reducing P content, along with increasing Ni content; and in Alloy 3 this was achieved by greatly reducing Sn content, slightly increasing P content and increasing Ni content, as compared to commercially available Meta-Braze™ 077.
- As-cast microstructures of the three developed alloys exhibited Cu-rich solid solution (globular for Alloys 1 and 2, continuous for Alloy 3), Cu-Sn-rich solid solution (diminished in Alloy 3), $Ni(Cu)_2P$ and eutectic Cu_3P. Similar Vickers hardness values were measured for all three alloys, with Alloy 3 being slightly softer owing to continuous solid solution phase.
- Inferior flowability and wetting of Alloys 1–3 as filler metals, compared to Meta-Braze™ 077, was observed in the joint, and as such joint widths remained large due to the initial thickness of melt-spun Alloy 1 – 3 foils, with weight of the upper base metal piece being insufficient to aid filling of the gap. Alloy 3 performed perhaps worst in this regard, while Alloy 1 achieved a joint gap closer in width to the joint using Meta-Braze™ 077. It is suggested that the reduction in Sn and P content caused inhibited flow of molten filler metal.
- Joints using Meta-Braze™ 077 and Alloy 2 had the lowest measured fractions of Cu-rich solid solution (0.61 and 0.66 respectively), while joints using Alloys 1 and 3 had the highest (0.78 and 0.77 respectively). Correspondingly, Vickers microhardness profiles suggested greater and more consistent ductility in the joints using Alloys 1 and 3 as filler metal. Alloy 3 performed well in this regard despite the joint width being the largest of all produced joints, and it is suggested that optimisation may lead to further improvement in performance,

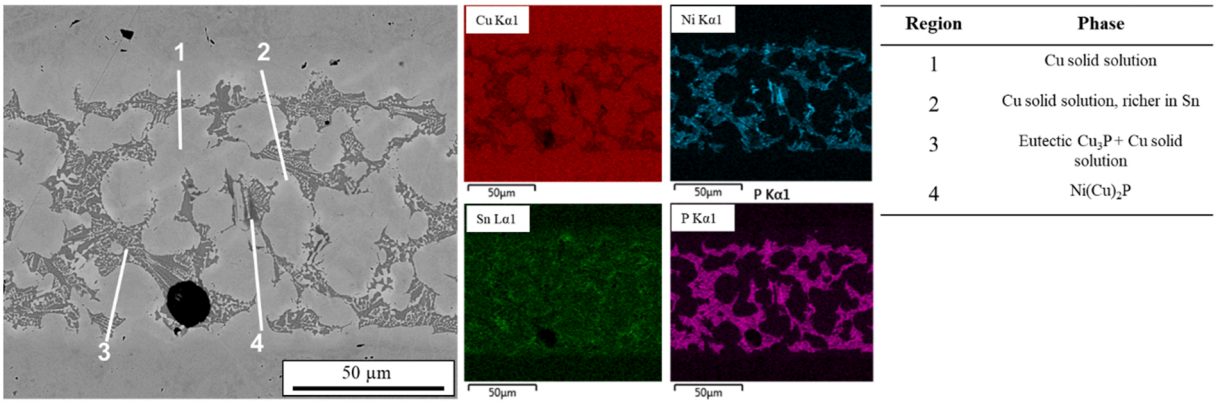

Fig. 17. SEM (BSE) image of Cu tokens joined using Alloy 1 as filler metal, along with EDS maps showing distribution of Cu, Ni, Sn, and P in the joint microstructure.

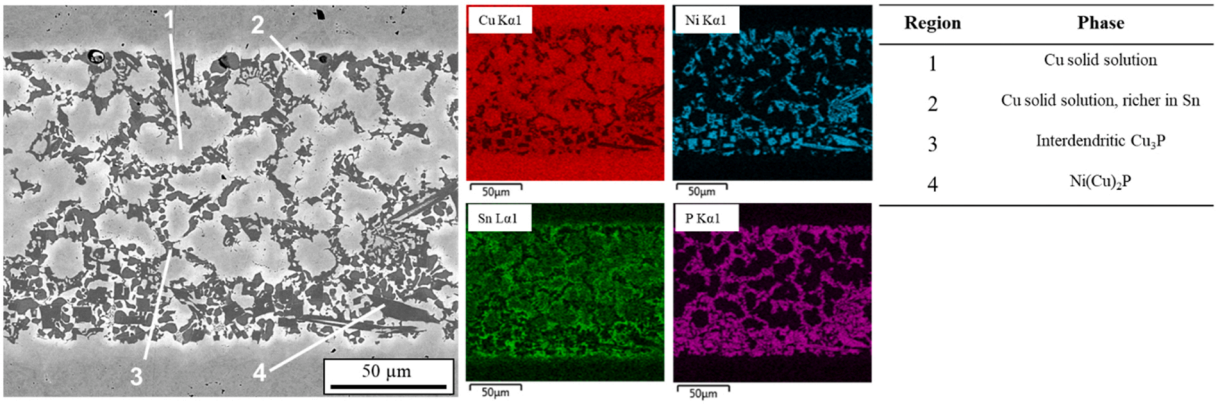

Fig. 18. SEM (BSE) image of Cu tokens joined using Alloy 2 as filler metal, along with EDS maps showing distribution of Cu, Ni, Sn, and P in the joint microstructure.

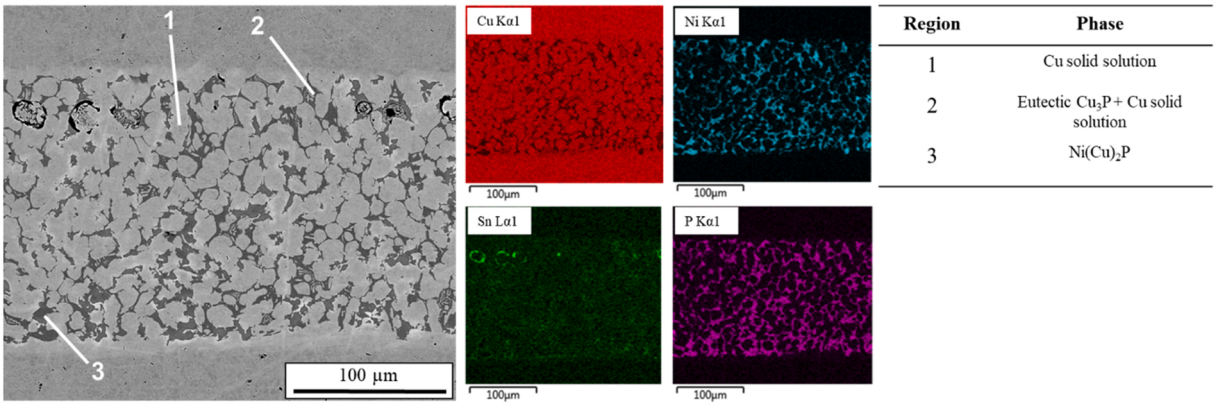

Region	Phase
1	Cu solid solution
2	Eutectic Cu_3P + Cu solid solution
3	$Ni(Cu)_2P$

Fig. 19. SEM (BSE) image of Cu tokens joined using Alloy 3 as filler metal, along with EDS maps showing distribution of Cu, Ni, Sn, and P in the joint microstructure.

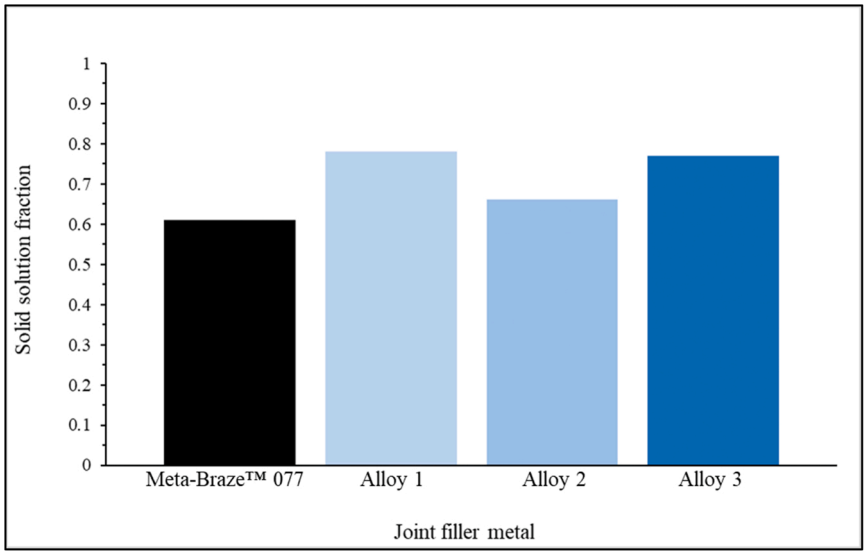

Fig. 20. Plot of solid solution fraction measured in joint section after brazing Cu with Meta-Braze™ 077 and melt-spun Alloys 1, 2 and 3, as determined by ImageJ software.

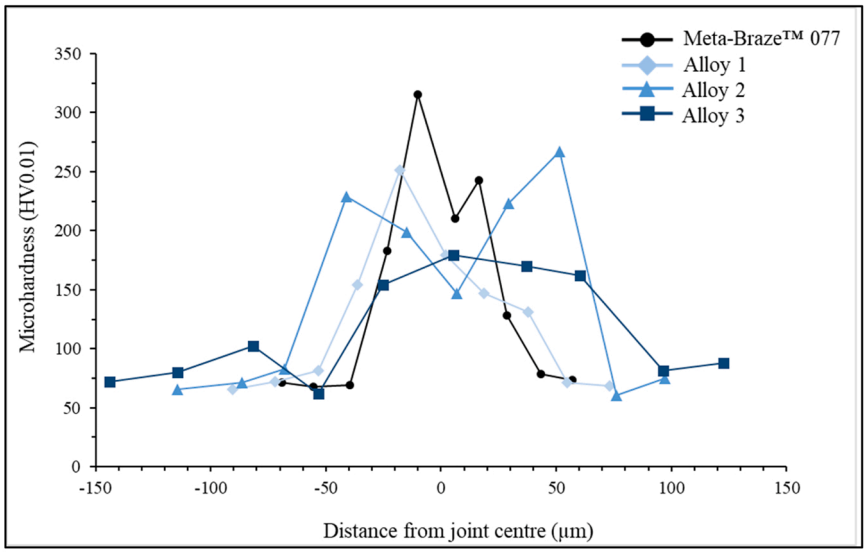

Fig. 21. Vickers microhardness (HV0.05) profiles of brazed joints using Meta-Braze™ 077 and Alloys 1 – 3 foils.

considering the possibly increased diffusion of P away from the joint region and thus increasing the fraction of solid solution.

CRediT authorship contribution statement

Liam Hardwick: Conceptualisation, Software, Investigation, Writing – original draft. **Phil Webb**: Resources, Writing – review & editing. **Russell Goodall**: Conceptualisation, Supervision, Funding acquisition, Writing – review & editing.

Declaration of Competing Interest

The authors declare that they have no known competing financial interests or personal relationships that could have appeared to influence the work reported in this paper.

Data availability

Data will be made available on request.

Acknowledgements

Funding: This work was supported by Research England [QR NPIF Award S12196] and UK Research and Innovation [EP/V050788/1]. For the purpose of open access, the author has applied a Creative Commons Attribution (CC BY) licence to any Author Accepted Manuscript version arising.

References

[1] M. Tajfar, E. Ganjeh, M.H. Mirbagheri, Evaluation of copper brazed joint failure by thermal-fatigue test applicable in heat exchangers, J. Alloy. Compd. 656 (2016) (2016) 347–356.
[2] A. Vazdirvanidis, S. Papadopoulou, S. Papaefthymiou, G. Pantazopoulos, D. Skarmoutsos, Copper tubing failure due to ant-nest corrosion, MATEC Web Conf. (2018) 188.
[3] Y.L. Shabtay, M. Ainali, A. Lea, New brazing processes using anneal-resistant copper and brass alloys, Mater. Des. 25 (1) (2004) 83–89.
[4] A. Lea, New brazing process uses anneal-resistant copper and brass alloys, MTZ Worldw. 64 (2003) 14–17.
[5] CuproBraze® Brazing Handbook, 8th ed..,, Luvata, Västerås, Sweden,, 2006.
[6] E. Lugscheider, O. Knotek, K. Klohn, Development of nickel-chromium-silicon base filler metals, Weld. Res. Suppl. (1978) 319–324.
[7] E. Lugscheider, O. Knotek, Brazing filler metals based on reacting Ni-Cr-B-Si alloys, Weld. Res. Suppl. (1976) 314–318.
[8] P. Jattakul, K. Kanlayasiri, Brazing of curved copper sheets using CuNiSnP amorphous filler metal, J. Alloy. Compd. 803 (2019) (2019) 610–617.
[9] N.A.M. Zahri, F. Yusof, Y. Miyashita, T. Ariga, A.S.M.A. Haseeb, N.H. Jamadon, et al., Brazing of porous copper foam/copper with amorphous Cu-9.7Sn-5.7Ni-7.0P (wt%) filler metal: interfacial microstructure and diffusion behavior. Welding in the World 64 (1) (2020) 209–217.
[10] M. Way, J. Willingham, R. Goodall, Brazing filler metals, Int. Mater. Rev. 65 (5) (2020) 257–285.
[11] A.M. Aminazad, A.M. Hadian, F. Ghasimakbari, Investigation on corrosion behaviour of copper brazed joints, Proc. Mater. Sci. 11 (2015) (2015) 672–678.
[12] Brazing — Filler metals (ISO 17672:2016) (2nd ed.). (2016). British Standards Institution.
[13] T. Noda, K. Oikawa, S. Itoh, M. Hino, T. Nagasaka, Thermodynamic evaluation of Cu-Cu3 P system based on newly determined Gibbs energy of formation of Cu3 P, Calphad: Comput. Coupling Phase Diagr. Thermochem. 33 (3) (2009) 557–560.
[14] W. Liu, S. Li, X. Li, X. Gao, Crystallization of amorphous Cu-6Ni-10Sn-7P alloy ribbons, J. Mater. Sci. Lett. 9 (1990) (1990) 904–905.
[15] J. Zhang, W. Yu, W. Lu, Mechanical properties and microstructure of pure copper joints brazed with amorphous Cu68.5Ni15.7Sn9.3P6.5 filler metal, Int. J. Simul. Syst. Sci. Technol. 17 (24) (2016) 19.1–19.5.
[16] H. Yu, Y. Sun, S.P. Alpay, M. Aindow, Microstructure effects in braze joints formed between Ag/W electrical contacts and Sn-coated Cu using Cu–Ag–P filler metal, J. Mater. Sci. 50 (1) (2015) 324–333.
[17] M.M. Sami, T. Zaharinie, F. Yusof, T. Ariga, Investigation on strength and microstructural evolution of porous cu/cu brazed joints using Cu-Ni-Sn-P filler, Metals 10 (2020) 3.
[18] A. Hasap, N. Noraphaiphipaksa, C. Kanchanomai, The microstructure and strength of copper alloy brazing joints, Weld. J. 93 (2014) 116–123.
[19] R.F. Sim, J.A. Willingham, Copper phosphorus based (self-fluxing) brazing alloys used for joining copper and its alloys. FWP, Journal 27 (1987) 33–39.
[20] A. Takeuchi, A. Inoue, Classification of bulk metallic glasses by atomic size difference, heat of mixing and period of constituent elements and its application to characterization of the main alloying element, Mater. Trans. 46 (12) (2005) 2817–2829.